Title

Unveiling the Indian Ocean forcing on winter eastern warming - western cooling pattern over North America.

Journal

Nature Communications, 15(1)

Authors

Hou, Yurong

Xie, Shang-Ping

Johnson, Nathaniel

et al.

Publication Date

2024-11-07

DOI

10.1038/s41467-024-53921-y

Peer reviewed

nature communications

Article

https://doi.org/10.1038/s41467-024-53921-y

Unveiling the Indian Ocean forcing on winter eastern warming – western cooling pattern over North America

Received: 22 February 2024

Accepted: 28 October 2024

Published online: 07 November 2024

Check for updates

Yurong Hou[1,2], Shang-Ping Xie[3], Nathaniel C. Johnson[4], Chunzai Wang[5,6], Changhyun Yoo[7], Kaiqiang Deng[8], Weijun Sun[9] & Xichen Li[1]

While the tropical Pacific teleconnection to North America has been studied extensively, the impact of the Indian Ocean on North American climate has received less attention. Here, through observational analysis and hierarchy atmospheric model simulations with different complexity, we find that the Indian Ocean plays a crucial role in North American winter climate through a teleconnection termed the Indian Ocean - North America pattern. We show that in the warm Indian Ocean phase, this teleconnection contributes to anomalously cold winters along the west coast of the United States through advection with increased mountain snowfall, while simultaneously leading to warmer conditions over the Great Lakes region. Snow-albedo feedback amplifies these Rossby wave-induced surface anomalies. Remarkably, this teleconnection pattern is at work on both interannual and multi-decadal time scales, with its climatic impact being slightly less pronounced than that induced by tropical Pacific sea surface temperature anomalies. Our findings underscore the significance of the Indian Ocean in both the prediction and future projection of North American climate.

In recent decades, severe cold spells and heavy snowfalls frequently struck North America in boreal winter[1–3]. In early 2023, record snowfall buried California towns at Mammoth Mountain, causing power outages for more than 100,000 residents. Exceptionally heavy snow and cold events also caused many serious problems by disrupting transportation, damaging agricultural production, and threatening public health and personal safety. It is thus important to investigate the main drivers and physical mechanisms of these cold events, and to further improve their prediction skills.

Recent studies have indicated that a series of physical mechanisms, including the atmospheric internal variability and regional feedbacks, may significantly influence the North American climate. For example, snow cover exerts an important effect on surface temperature anomalies over North America through snow-albedo feedback[4,5], while cloud feedback plays a crucial role in modulating the surface temperature via its radiative effects[6,7]. Furthermore, atmospheric internal variability is also important for mid-latitude temperature and precipitation variability over North America[8–11].

Remote forcings from the tropics and the Arctic also play pivotal roles in driving climate variations across North America by influencing atmospheric circulations. The tropical-extratropical teleconnection, recognized for over four decades, has been a focal point in climate

[1]International Center for Climate and Environment Sciences, Institute of Atmospheric Physics, Chinese Academy of Sciences, Beijing, China. [2]University of Chinese Academy of Sciences, Beijing, China. [3]Scripps Institution of Oceanography, University of California San Diego, La Jolla, CA, USA. [4]Geophysical Fluid Dynamics Laboratory, National Oceanic and Atmospheric Administration, Princeton, NJ, USA. [5]State Key Laboratory of Tropical Oceanography, South China Sea Institute of Oceanology, Chinese Academy of Sciences, Guangzhou, China. [6]Global Ocean and Climate Research Center, South China Sea Institute of Oceanology, Chinese Academy of Sciences, Guangzhou, China. [7]Department of Climate and Energy Systems Engineering, Ewha Womans University, Seoul, South Korea. [8]School of Atmospheric Sciences, Sun Yat-sen University, Zhuhai, China. [9]College of Geography and Environment, Shandong Normal University, Jinan, China. e-mail: lixichen@mail.iap.ac.cn

dynamics research, examining how changes in tropical oceans affect extratropical atmospheric circulation over both hemispheres[12,13]. The tropical Pacific sea surface temperature (SST) variability[14], particularly the El Niño-Southern Oscillation (ENSO), significantly impacts North American winter climate via the Pacific-North America (PNA) teleconnection pattern[15–17]. During the positive phase of PNA, often associated with the warm phase of ENSO, North America experiences a marked temperature contrast, with cold-air outbreaks in the southeast and warmer air in the northwest[18]. Moreover, SST anomalies in the tropical[19] and North Atlantic[20,21] contribute to North American climate variability by altering large-scale atmospheric circulation through Rossby wave dynamics, while sea-ice loss over the Barents-Kara Seas usually heats the North American continent through thermal advection[22].

In addition, numerous studies have investigated Rossby wave trains generated by heat sources across the Indo-Pacific Oceans and their impacts on climate patterns over the Northern Hemisphere[23–27]. On intraseasonal time scales, convective activities in the tropical Indo-Pacific Oceans during different phases of the Madden-Julian Oscillation (MJO) can trigger Rossby wave trains[28], which propagate toward the North Pacific and North America, contributing to surface temperature and precipitation anomalies in these regions[29–31]. Based on Rossby wave dynamics[32–35], similar teleconnection patterns also work for interannual and longer time scales. However, the interannual variability over the Indian Ocean is often considered less important than ENSO events in affecting North American climate, partly due to the strong interaction between the Indian Ocean Basin Mode (IOBM)[36,37] and ENSO[16,38–40]. An El Niño episode typically drives a warm anomaly over the Indian Ocean from early winter through the following summer[41], which may obscure the Rossby wave train induced by Indian Ocean warming and the ENSO-related PNA pattern[42–45]. As a result, the remote impact of Indian Ocean warming has long been viewed as a passive effect of ENSO events.

Here, we aim to isolate the impact of Indian Ocean warming on the North American climate from the ENSO-induced teleconnections, further clarifying the effects of regional feedbacks. Our statistical analyses and numerical model simulations reveal that Indian Ocean warming can generate a stationary Rossby wave train, driving seesaw-like variations in SAT and snowfall across the North American continent, with snow-albedo feedback amplifying this process. Overall, the impact of Indian Ocean warming on the North American winter climate is comparable to, or even greater than, that of ENSO in some regions, especially along the densely populated and economically developed west and east coasts.

Results

The Indian Ocean – North America teleconnection pattern

We first retrieve the North American winter (December-January-February, DJF) SAT anomalies associated with the IOBM index (Supplementary Fig. 1b) through linear partial regression analysis using the ERA5 reanalysis dataset. Linear trends and the Niño 3.4 index have been removed prior to the regression analysis to isolate the impact of the Indian Ocean on North America. The results show that the Indian Ocean warming can trigger a western cooling - eastern warming pattern over North America (Fig. 1a), characterized by significant cooling over Alaska and the western United States, extending from the west coast to the eastern edge of the Rocky Mountain (about 100°W). In contrast, a warming signal is observed over northeastern North America, particularly across Quebec and the Great Lakes region.

We find the same western cooling - eastern warming anomalies over the North American continent when repeating the regression analysis with four additional state-of-the-art reanalysis datasets: JRA55, MERRA2, NCEP2 and CFSR (Supplementary Fig. 2). To further assess the robustness of this linkage, we select three regions – the west coast (blue box in Fig. 1a), the east coast (red box), and Alaska (cyan box) – and quantify the Indian Ocean-induced cooling and warming signals over these areas using the five reanalysis datasets (Fig. 2a). Across all datasets, Indian Ocean warming consistently drives significant warming over eastern North America (Fig. 2a, bottom panel), and significant cold anomalies over Alaska and the west coast (Fig. 2a, upper and middle panels). Specifically, one standard deviation of the Indian Ocean basin warming is associated with a 0.69–0.73 °C increase in temperature (among the five reanalyses) over the east coast of North America, a 0.41–0.56 °C decrease over the west coast, and approximately a 1.01–1.2 °C decrease over Alaska.

This Indian Ocean-induced seesaw-like SAT anomaly is accompanied by a contrasting snowfall pattern over North America (Fig. 1b), with heavier snowfall in northern California, Oregon, Washington, and southwestern British Columbia, but reduced snowfall over broader regions, including the Great Lakes. Particularly, one standard deviation of the IOBM index corresponds to an increase of up to 12 mm in snowfall (water equivalent) along the west coast of the United States during the winter season (Fig. 1b). The anomalies in SAT and snowfall further lead to snow cover changes over the North American continent (Fig. 1c), contributing to a 3% increase (by area) in snow cover over western North America (blue box in Fig. 1c), but a 2% decrease around the Great Lakes region (red box).

In order to validate the robustness of the impacts of Indian Ocean on North American winter climate, we applied both the Student's *t*-test and a more stringent field significance test[46] on the regression results for SAT and snow cover. All SAT and snow cover regression results over the west and east coasts of the North America can pass the Student's *t*-test (indicated by magenta plus signs in Fig. 1a, c). Furthermore, the SAT regression results for the west (cyan box) and east (red box) coasts, as well as Alaska (blue box), also passed the field significance test (black circles in Fig. 1a), while the snow cover regression results for the west coast (blue box) of the United States also passed the field significance test (black circles in Fig. 1c). These findings highlight the robustness of the linkage between the Indian Ocean and North American winter climate, especially along the west coast of the United States.

To further identify the impact of Indian Ocean warming on North American climate and compare it with that of ENSO events, we evaluate the effect of the Niño 3.4 index on North American SAT through linear regression analysis (Supplementary Fig. 3). Consistent with previous studies[47,48], the warming in the equatorial Pacific and its associated PNA-like pattern typically produce a northern warming-southern cooling pattern over the North American continent (Supplementary Fig. 3a). This temperature distribution is distinct from the Indian Ocean warming-induced western cooling - eastern warming pattern. One standard deviation of the Niño 3.4 index is associated with a 0.89 °C warming (bottom panel in Supplementary Fig. 4a) over the northern parts of North America (red box in Supplementary Fig. 3a), but a 0.32 °C cooling (upper panel in Supplementary Fig. 4a) over southern regions (blue box in Supplementary Fig. 3a). This suggests that the amplitude of the Indian Ocean-induced temperature anomaly is only slightly smaller than that of the ENSO-induced anomaly. In addition, although the area influenced by the Indian Ocean is relatively small (Fig. 1a and Supplementary Fig. 3a), it encompasses the west coast and the Great Lakes region, both of which are densely populated economic and industrial hubs.

Climate teleconnections are often mediated by large-scale atmospheric circulation adjustments, especially through Rossby wave dynamics[15,17]. To further clarify the physical pathway of the Indian Ocean - North America (INA) teleconnection, we conduct partial regression analysis of sea level pressure (SLP, shading in Fig. 3c) and geopotential height (GPH) at 200-hPa (Fig. 3a) and 500-hPa (Fig. 3b) levels against the IOBM index in winter. The negative anomalies of the observed outgoing longwave radiation related to Indian Ocean warming (light blue contours in Fig. 3c) indicate intensified tropical

https://doi.org/10.1038/s41467-024-53921-y

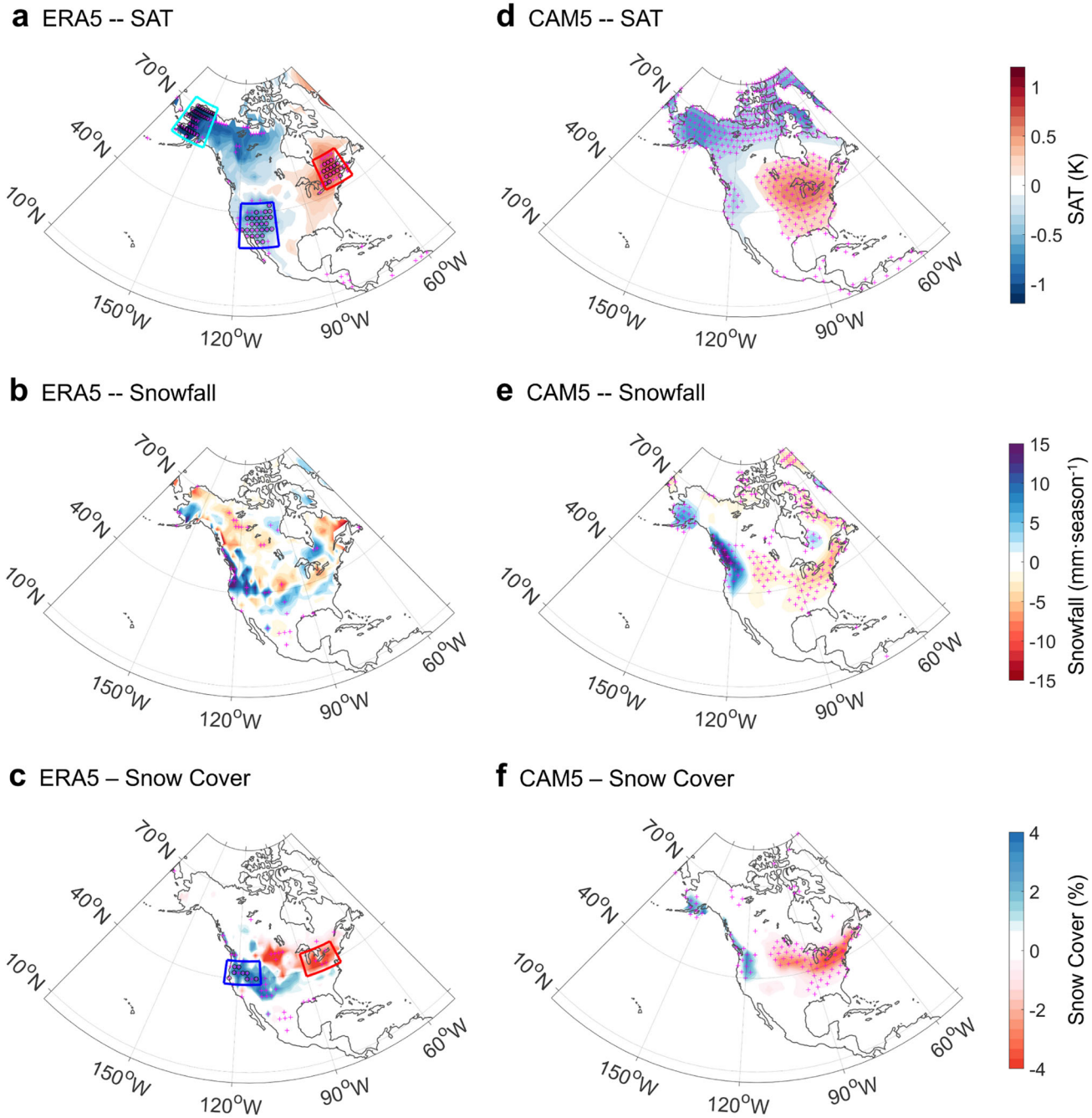

Fig. 1 | Indian Ocean warming – induced North American wintertime (December–January–February, DJF) climate anomalies retrieved from ERA5 reanalysis dataset and simulated in CAM5 model experiment. a–c Partial regressions of DJF North American surface air temperature (SAT, **a**), snowfall (**b**), and snow cover (**c**) against the normalized Indian Ocean Basin Mode (IOBM) index during the 1979-2020 period, with the Niño 3.4 index removed. **d–f** The simulated responses of DJF SAT (**d**), snowfall (**e**), and snow cover (**f**) in the CAM5 ensemble model experiment, only driven by the observed tropical Indian Ocean sea surface temperature variability. The magenta plus signs represent the areas with statistically significant regression coefficients at a level of <10% based on Student's *t* test. The black circles in **a** and **c** signify locally significant grid points at the same significance level through controlling false discovery rate (see Methods). Three regions with pronounced SAT variations are selected in **a** over the west coast (blue box, 119°W-104°W, 28°N-43°N), the east coast (red box, 79°W-65°W, 42°N-53°N), and over Alaska (cyan box, 168°W-145°W, 59°N-72°N) to quantify. The blue box (126°W-110°W, 38°N-46°N) and the red box (90°W-74°W, 38°N-46°N) in **c** indicate the areas with significantly increased and decreased snow cover, respectively.

convection in the western Indian Ocean. The convective heating drives atmospheric circulation anomalies, with a strong barotropic structure in the extratropics (Fig. 3a–c), manifesting as a Rossby wave train along the great circle originating from the Indian Ocean to North America (dashed arrow in Fig. 3a). To trace the propagation of this stationary Rossby wave train, we diagnosed the anomalous wave flux activity at 200 hPa associated with the tropical Indian Ocean warming (Supplementary Fig. 5). The pathway of the wave train is influenced by the waveguide effect of the Asian-Pacific jet[49]. In addition, the wave train is further amplified near the international dateline (Supplementary Fig. 5) due to barotropic instability in the jet exit region[12,33]. In the lower troposphere (Fig. 3c), the circulation adjustment is characterized by an anomalous high-pressure center over the mid-latitude North Pacific, extending from the Sea of Japan to the west coast of the United

https://doi.org/10.1038/s41467-024-53921-y

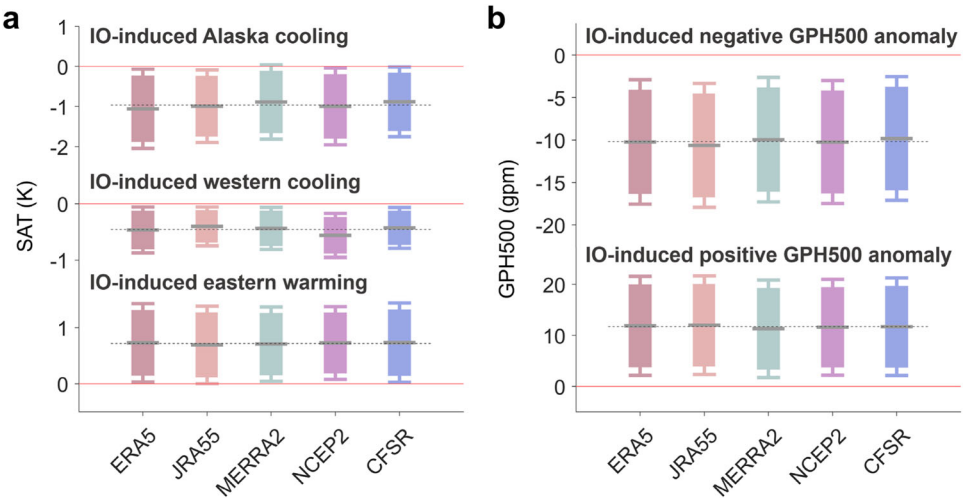

Fig. 2 | Statistics of the Indian Ocean warming-induced North American surface air temperature (SAT) and geopotential height at 500 hPa (GPH500) anomalies in five state-of-the-art reanalysis datasets. a Wintertime (December-January-February, DJF) Indian Ocean warming-induced western cooling (blue box in Fig. 1a), Alaska cooling (cyan box in Fig. 1a), and eastern warming (red box in Fig. 1a), calculated by the partial regressions of area averages against the normalized Indian Ocean Basin Mode (IOBM) index, with the Niño 3.4 index removed. Short solid gray lines represent regression coefficients in each reanalysis, long dotted gray lines represent regression coefficients of the ensemble mean of the five reanalyses, thick bars represent the 90% confidence interval of each reanalysis, and error bars represent the 95% confidence interval of each reanalysis. Statistical characteristics of different reanalysis datasets are illustrated by different colors. **b** Indian Ocean warming-induced positive anomalies of the GPH500 over the mid-latitude North Pacific (red box in Fig. 3b) and negative anomalies over North America (blue box in Fig. 3b) in DJF.

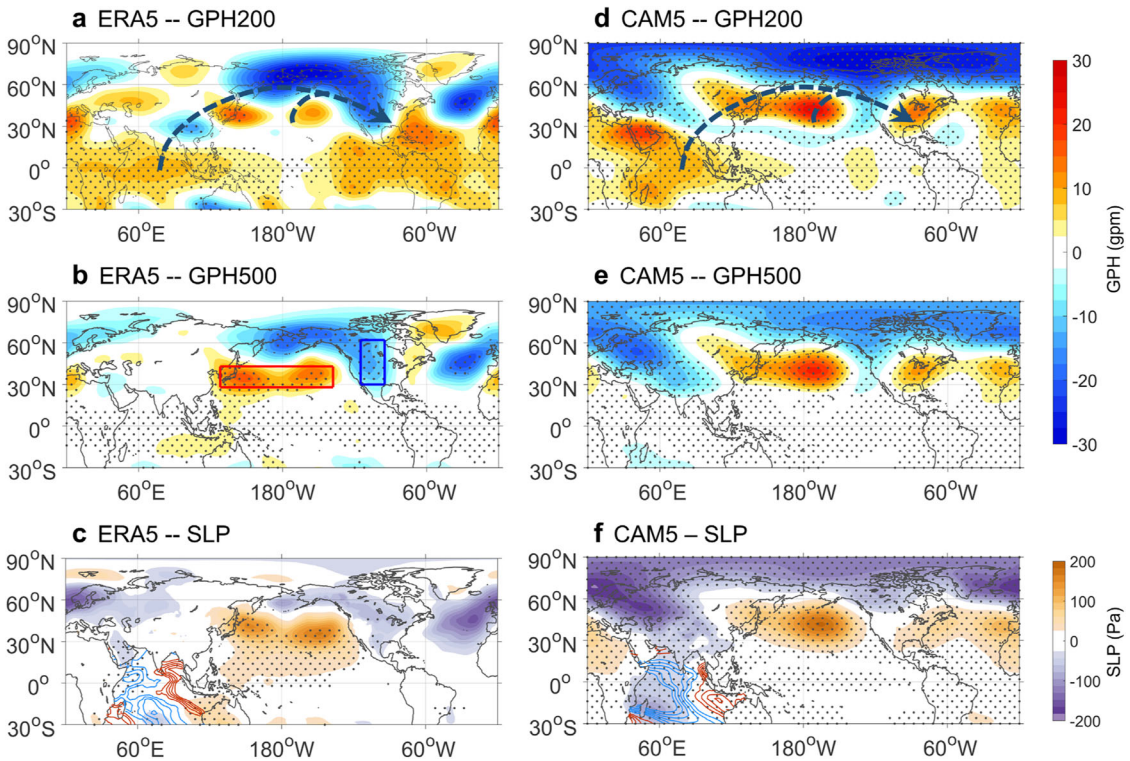

Fig. 3 | Indian Ocean warming – induced wintertime (December-January-February, DJF) atmospheric circulation anomalies from ERA5 and simulated in CAM5 experiment. Partial regression coefficients of DJF geopotential height at 200 hPa (GPH200, **a**) and 500 hPa (GPH500, **b**) and sea level pressure (SLP, **c**) against the normalized Indian Ocean Basin Mode (IOBM) index in the ERA5 reanalysis dataset, with the Niño 3.4 index removed. Model responses of GPH200 (**d**), GPH500 (**e**) and SLP (**f**) in the CAM5 ensemble experiment driven by the tropical Indian Ocean warming. Contours in panels **c** and **f** over the Indian Ocean show the regression pattern of the observed and simulated outgoing longwave radiation (OLR) onto the normalized IOBM index. Light blue (orange) contours at 1 W·m^{-2} intervals show negative (positive) OLR anomalies. Stippling represents the areas with statistically significant regression coefficients at a level of <10% based on Student's *t* test. The Indian Ocean warming-induced circulation patterns are barotropic from the surface to 200 hPa, exhibiting strong coherent features between the reanalysis data (**a**–**c**) and the atmospheric model (**d**–**f**). Dashed arrows in **a** and **d** highlight the Rossby wave train linking the Indian Ocean and North America.

States, and an anomalous low-pressure center covering the Bering Sea, Alaska, and western Canada.

Remarkably, the INA pattern is robust across all five reanalysis datasets (Supplementary Figs. 6 and 7). Statistical analysis indicates that the Indian Ocean warming may contribute to an increase of 11.3–12.1 gpm in geopotential height at 500 hPa over the mid-latitude North Pacific (red box in Fig. 3b) and a decrease of 9.8–10.6 gpm over North America (blue box in Fig. 3b) among the five reanalysis datasets (Fig. 2b). The atmospheric circulation adjustment further contributes to the SAT and snowfall anomalies through thermal advection.

Reproducing the INA teleconnection by numerical model experiments

Although the statistical analysis reveals the linkage between the tropical Indian Ocean and North American climate, it does not identify a causal relationship. For instance, Kumar and Hoerling[42] argued that Indian Ocean SST anomalies are induced by ENSO, incapable of inducing an atmospheric response. Furthermore, the linear assumption adopted in partial regression analysis may not be valid, raising questions about the linear decomposition of the Indian Ocean's effects from those of the Pacific. To further clarify causality and isolate the impact of the Indian Ocean, we conduct an ensemble model experiment using the Community Atmospheric Model (CAM5), driven only by the observed Indian Ocean SST variability from 1979 to 2020 (see Methods). We then regress the simulated North American SAT against the IOBM index. The simulated SAT response is very similar to that of the partial regression analysis (Fig. 1a), with cold anomalies over Alaska and the west coast of the United States, as well as warm anomalies over the eastern half of North America (Fig. 1d). The numerical model experiment also well reproduces the east-west contrast in snowfall and snow cover (Fig. 1e, f), showing heavier snow over the west coast and lighter snow in eastern North America, especially around the Great Lakes.

Despite a strong similarity in regression patterns between reanalysis datasets and model simulation, the SAT pattern in response to the Indian Ocean warming in the CAM5 experiment exhibits a westward shift in comparison to that in the partial regression analysis. In the simulation, the cold anomaly over mid-latitude North America is confined to a narrow band near the west coast of the United States (Fig. 1d), while the warm anomaly extends from the east coast to central North America (Fig. 1d). Similar westward shifts are also seen in the simulated snowfall and snow cover patterns (Fig. 1e, f). Notably, in both the reanalyses and numerical model experiment, the west coast of North America consistently experiences anomalously severe winters and heavier snowfall in response to the Indian Ocean basin-scale warming.

Importantly, the numerical experiment well simulates the Indian Ocean-induced Rossby wave train. The regression patterns of simulated SLP and GPH at multiple pressure levels (Fig. 3d–f) against the IOBM index reveal a stationary Rossby wave pattern from the tropical Indian Ocean to North America (Fig. 3d). Its three-dimensional structure (Fig. 3d–f) closely resembles the partial regression patterns in the reanalysis datasets (Fig. 3a–c). The anomalous tropical convection in the experiment (light blue contours in Fig. 3f), driven by Indian Ocean SSTs, generates a stationary Rossby wave train propagating poleward and eastward to the North Pacific and North America, forming an anomalous high-pressure center over the mid-latitude North Pacific and a low-pressure center across the North American continent (Fig. 3d–f), albeit with a slight westward shift of the wave train and an excessively strong response over the Arctic compared to the reanalyses. We note that there are other mechanisms possibly working to form the Rossby wave response. For example, the barotropic energy conversion from the subtropical jet to the eddy field likely amplifies the response, primarily in regions of strong climatological deformation[12]. Also, the synoptic transient eddies may feed back into the linear Rossby wave response to Indian Ocean warming[13]. These two mechanisms are resolved in the CAM5 simulation. Nonetheless, it will be shown later that the stationary Rossby wave response can be reproduced in an initial value calculation of GFDL dry dynamical core. The shift in the circulation pattern also contributes to the westward shift of the seesaw-like SAT and snowfall patterns in simulation results through the adjustment of thermal advection.

Over the past half-century, the Indian Ocean has experienced rapid and steady warming[50], which may potentially drive multi-decadal changes in the global climate system through atmospheric bridges involving the INA pattern. However, this multi-decadal impact could be overwhelmed by other climate factors, such as the global warming signal[51] and the global impacts of the Pacific[52,53] and Atlantic[54,55] Oceans. As a result, it may be challenging to identify the Indian Ocean-induced teleconnection signal from observational and reanalysis datasets. Nevertheless, the ensemble model experiment provides a valuable reference for isolating the multi-decadal climate response to Indian Ocean warming.

We thus illustrate the multi-decadal trends of SLP, GPH, and SAT (Supplementary Fig. 8) in the CAM5 experiment forced by Indian Ocean SSTs. These results show that, on multi-decadal time scales, the Indian Ocean warming can trigger a stationary Rossby wave train, whose horizontal pattern is nearly identical to that of the INA teleconnection pattern on interannual time scales. The convective heating anomalies in the Indian Ocean generate an anomalous high-pressure center over the mid-latitude North Pacific (Supplementary Fig. 8b–d) and a low-pressure center over western Canada, leading to cooling in Alaska and along the west coast of North America, meanwhile warming the central-eastern regions of the continent (Supplementary Fig. 8a).

The simulation results indicate that the INA pattern works on both interannual and multi-decadal time scales, contributing to recent multi-decadal climate changes. Our findings thus qualitatively demonstrate the effects of the Indian Ocean warming on climate variations over the North Pacific and North America. In view of the complexity of the Earth's climate system, this result also underscores the urgent need to quantify the impact of the Indian Ocean warming and to further clarify its interactions with changes in other ocean basins.

Given that the source of the Rossby wave train is not fully isolated in the partial regression analysis of reanalysis data (Fig. 3a) or in the simulated regression pattern (Fig. 3d), we further simulate the evolution of the atmospheric circulation response to the Indian Ocean forcing during winter using an idealized atmospheric model, the GFDL dry dynamical core, to clarify the physical dynamics. In this simulation, the model is perturbed by an idealized convective heating over the tropical Indian Ocean, while the winter climatological basic state is maintained as a balanced state of the model's governing equations (see Methods). The experimental design has been employed to study the atmospheric response to a thermal forcing[56–58]. The model simulation illustrates a clear picture of the INA pattern (Supplementary Fig. 9), demonstrating that convective heating over the tropical Indian Ocean triggers a stationary Rossby wave train, which propagates along a great circle linking the Indian Ocean to North America. In addition to this direct pathway, another wave source appears in the subtropical North Pacific near the international dateline, which reflects the barotropic instability in the jet exit region[12], thus intensifying the stationary wave train and forming a teleconnection pattern similar to those in the reanalysis dataset (Fig. 3a) and the CAM5 model simulation (Fig. 3d), albeit with a slight phase shift in the wave trains.

The coherence between the reanalysis datasets (Fig. 3a), the comprehensive atmospheric model (Fig. 3d), and the idealized atmospheric model (Supplementary Fig. 9) verifies the robustness of the INA teleconnection pattern. These results reveal that the Indian Ocean heating contributes to the large-scale circulation adjustment over the North Pacific and North America through Rossby wave dynamics,

https://doi.org/10.1038/s41467-024-53921-y

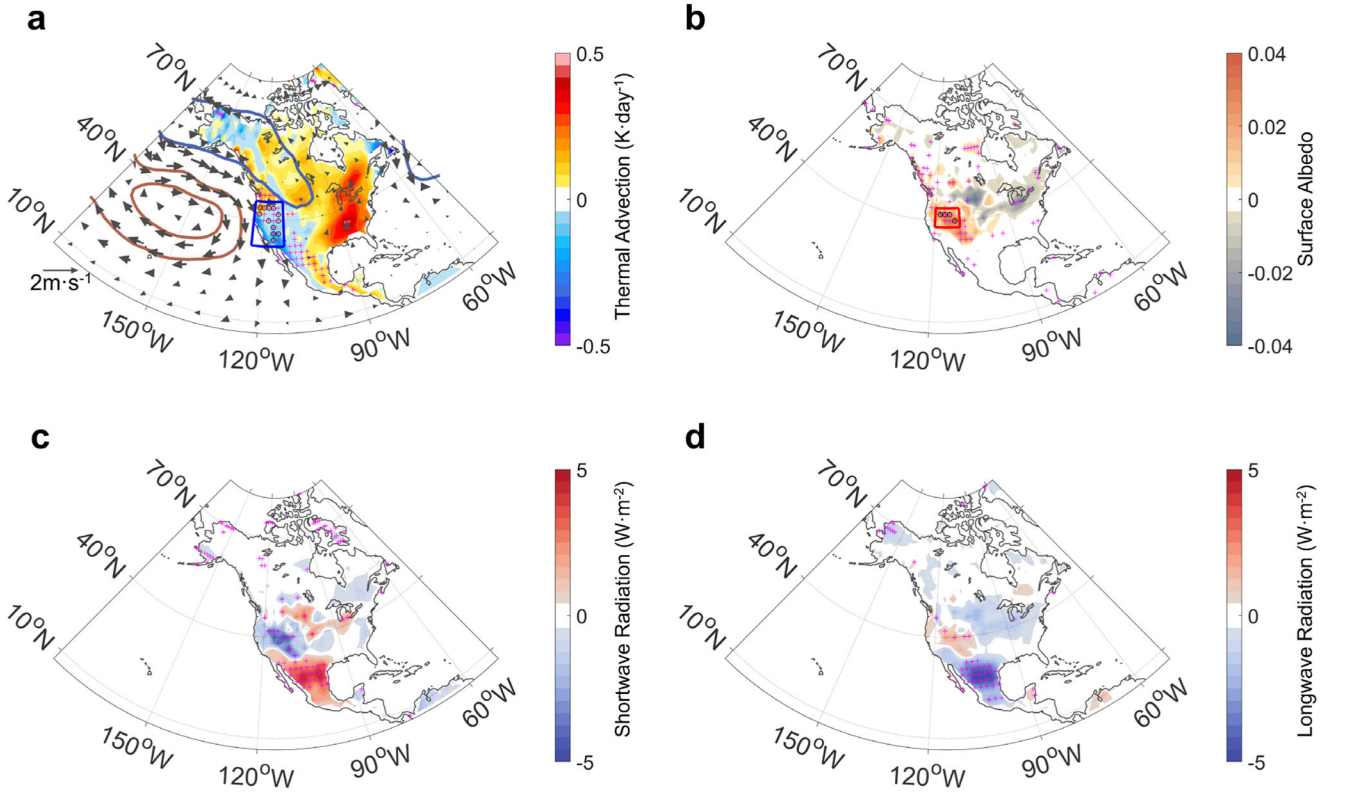

Fig. 4 | Thermal advection, surface albedo and surface radiation flux over North America from ERA5 dataset associated with the Indian Ocean warming in winter (December-January-February, DJF). a Partial regression patterns of thermal advection (color shading), together with the geopotential height (contours) and wind (vectors) anomalies at the 850-hPa level against the normalized Indian Ocean Basin Mode (IOBM) index in DJF, with the Niño 3.4 index removed. Red (blue) contours at 5 gpm intervals show positive (negative) anomalies. Same as panel **a**, but for the surface albedo (**b**), the surface net shortwave radiation (**c**), and the surface net longwave radiation (**d**). The magenta plus signs indicate the areas with statistically significant regression coefficients at a level of <10% based on Student's *t* test. The black circles in **a** and **b** represent locally significant grid points at the same significance level through controlling false discovery rate (see Methods).

leading to temperature and snowfall changes across the North American continent in winter.

Physical mechanisms for North American response

Our statistical analysis and numerical model simulation suggest that the Indian Ocean warming can drive a pair of anomalous high- and low-pressure centers over the mid-latitude North Pacific and North America (Fig. 3). The circulation adjustment further induces changes in SAT and snow cover in North America. Here, we evaluate the physical mechanisms involved in this process. We first illustrate the thermal advection anomaly at the 850-hPa level (color shading in Fig. 4a) associated with the Indian Ocean warming using linear partial regression analysis on the ERA5 dataset, together with the GPH and wind anomalies at the same pressure level (contours and vectors in Fig. 4a). These results show that the anticyclonic circulation anomaly over the mid-latitude North Pacific drives anomalous cold advection toward the west coast of North America, while the cyclonic circulation anomaly across western Canada induces anomalous warm advection in central-eastern North America, thereby contributing to the western cooling - eastern warming pattern.

We further calculate each term of the surface energy budget related to the Indian Ocean warming. The large-scale atmospheric circulation anomalies forced by the Indian Ocean warming may not induce prominent changes in local sensible and latent heat fluxes over North America in winter, as these signals are relatively weak and statistically insignificant across most of the continent (not shown). In contrast, the radiation anomalies play a key role in driving North American wintertime SAT changes. The surface net shortwave radiation (Fig. 4c, positive downward) decreases significantly by approximately 2.2 $W \cdot m^{-2}$ from the west coast of the United States to the eastern edge of the Rocky Mountains in response to one standard deviation of the Indian Ocean basin warming, which likely contributes to the cooling signal in this region (Fig. 1a). The longwave radiation anomaly induced by Indian Ocean warming (Fig. 4d) is relatively smaller, with a spatial distribution opposite to that of the shortwave radiation, partially offsetting its effects (Fig. 4c).

We further investigate regional feedbacks involved in these radiation changes. Previous studies have shown that cloud feedback[6,7] and snow-albedo feedback[4,5] can facilitate the temperature anomalies through local radiation effects. Hence, we examine the cloud cover changes in response to Indian Ocean warming through partial regression analysis (Supplementary Fig. 10). We also calculate the Indian Ocean warming-induced surface albedo anomalies over North America (Fig. 4b) and compare them with the spatial patterns of the surface net shortwave radiation anomaly (Fig. 4c) and the snow cover anomaly (Fig. 1c).

The cloud cover anomaly induced by Indian Ocean warming does not exert a dominant influence on radiation flux changes over most of the United States (Supplementary Fig. 10). However, the atmospheric circulation adjustment over the North Pacific and North America related to Indian Ocean warming enhances moisture convergence (not shown) over northern Mexico. This provides favorable conditions for increased cloud cover and resultant changes in longwave (Fig. 4d) and shortwave (Fig. 4e) radiation fluxes in this region. While these radiative effects offset each other and do not result in a pronounced SAT anomaly over Mexico (Fig. 1a), the effect of cloud feedback is limited in

areas where significant Indian Ocean-induced SAT changes occur over North America.

Notably, the snow-albedo feedback appears to play an important role in cooling the western parts of the United States (Fig. 1a). The Indian Ocean warming drives increased snow cover over mid-latitude North America (Fig. 1c), extending from the west coast of the United States to the Rocky Mountains. The enhanced snow cover leads to higher surface albedo over the same area (Fig. 4b) and associated increased upward shortwave radiation, further contributing to a reduction in surface net shortwave radiation in the western United States (Fig. 4c). The close correspondence among the spatial patterns of snow cover, surface albedo, and surface shortwave radiation emphasizes the importance of snow-albedo feedback in cold anomalies over the western United States (Fig. 1a), in response to the Indian Ocean-induced teleconnection.

On the other hand, the surface cooling may in return slow the melting of snow over mid-latitude North America. This positive feedback amplifies the effect of the cold advection driven by the Indian Ocean warming-induced circulation anomalies (Fig. 4a), leading to more pronounced cooling over the western United States (Fig. 1a).

Discussion

In this study, we have singled out the INA teleconnection pattern and further clarify its associated climate impacts on North America (Fig. 5). The Indian Ocean basin warming generates a stationary Rossby wave train linking the Indian Ocean to North America in winter (thick gray arrows in Fig. 5), establishing an anomalous high-pressure center over the mid-latitude North Pacific and an anomalous low-pressure center over Alaska and western Canada. The resulting large-scale atmospheric circulation changes drive a seesaw-like SAT pattern across the North American continent (blue and red shadings in Fig. 5) through thermal advection, with cold anomalies over the western United States and Alaska, but warm anomalies in central-eastern North America. The temperature variations are accompanied by increased snowfall along the west coast of mid-latitude North America, while snow cover changes (white shading in Fig. 5) interact with the SAT through snow-albedo feedback, further amplifying this seesaw-like temperature pattern.

Atmospheric teleconnection patterns linking climate variabilities between the tropics and extratropics have been extensively studied since the late 20th century[15,59,60]. In particular, the intraseasonal variability over the tropical Indo-Pacific Oceans, such as the MJO, may largely contribute to North American intraseasonal climate variations[29–31]. Similar teleconnection mechanisms, based on Rossby wave dynamics, also operate on interannual and longer time scales[32–35]. However, their specific impacts on North American climate remain unclear. In addition, the influence of Indian Ocean SST variability on North American climate has often been considered as secondary, due to the strong correlation between ENSO and IOBM events, which confounds the Indian Ocean-induced teleconnection with that induced by the tropical Pacific-induced PNA pattern[43–45]. This study isolates the remote effects of Indian Ocean warming through both observational statistical analysis and numerical model experiments. The mutually consistent results reemphasize the robustness of the INA teleconnection pattern, which, despite being somewhat weaker in magnitude, is comparable to the tropical Pacific-induced PNA pattern.

This teleconnection pattern drives cold winters over the west coast of North America, including northern California, Oregon, Washington, and British Columbia, accompanied by snowfall increases of up to 12 mm (water equivalent). This has broad societal implications, potentially affecting transportation, energy supply, agricultural production, and public health in these regions. Given that these areas are densely populated and key hubs of agriculture and industry, the Indian Ocean-induced teleconnection pattern revealed in this study could have an outsized economic impact on North America.

This study elucidates the effects of the INA pattern, which affects the global atmospheric circulation on both interannual and decadal time scales. This teleconnection pattern serves as an element within the intricate and interactive climate system. On interannual time scales, it interacts with the tropical Pacific-induced PNA pattern[43–45],

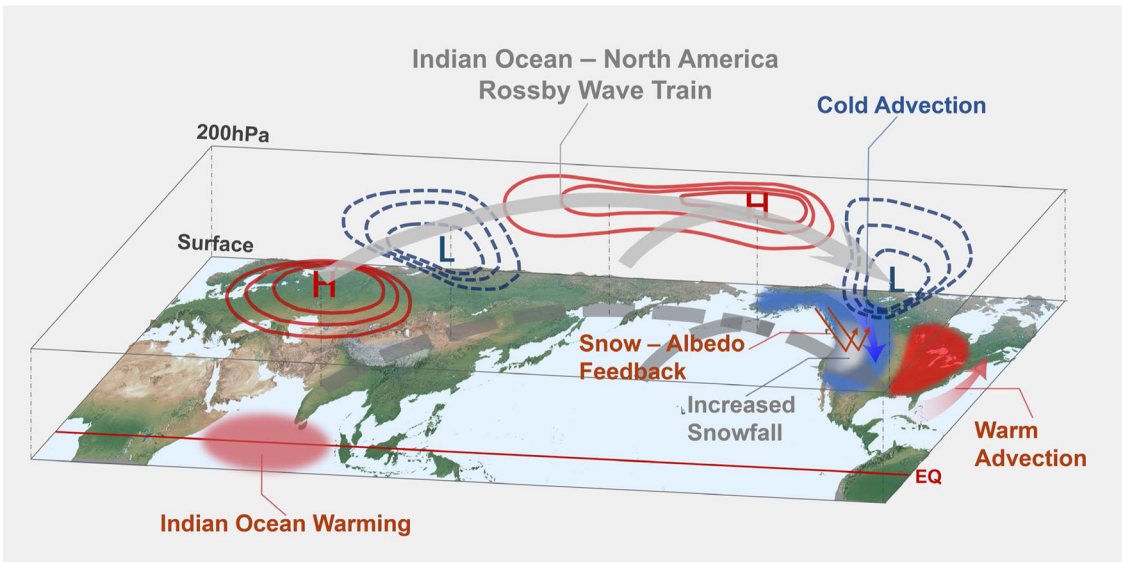

Fig. 5 | Schematic diagram of Rossby wave train linking the Indian Ocean and North America, and its impacts on North American temperature and snowfall. The Indian Ocean warming (light red shading) triggers a stationary Rossby wave train (thick gray arrows) propagating poleward and eastward in boreal winter, forming an anomalous high-pressure center over the mid-latitude North Pacific (red contours) and an anomalous low-pressure center across Canada (blue contours). The Indian Ocean warming-induced large-scale atmospheric circulation adjustment further drives an eastern warming (dark red shading) - western cooling (blue shading) temperature pattern over North America through thermal advection. Temperature changes are accompanied by increased snowfall over the high elevations of the west coast of the United States (gray shading). The snow cover anomaly (white shading) further amplifies surface temperature changes through snow-albedo feedback.

while on decadal and longer time scales, it works together with other teleconnection patterns originating from the Pacific[51], Atlantic[54], and Arctic[61], all contributing to observed circulation changes. While this study clarifies the spatial pattern and physical processes of the Indian Ocean-induced teleconnection, the relative importance of and interactions among various teleconnections, and their implications for seasonal-to-decadal climate prediction, still require further investigation, which will be a main focus of our future work.

Methods

Datasets

We employ the SST data for the period 1979–2020 from the Met Office Hadley Centre Global SST dataset (HadISST)[62] in the statistical analyses and numerical model simulations (serving as the lower boundary forcing). The outgoing longwave radiation data[63] from National Oceanic and Atmospheric Administration is utilized to examine the tropical convection anomalies. We obtain monthly mean atmospheric variables during 1979–2020, including SAT, SLP, and GPH, etc., from five state-of-the-art reanalysis datasets: (1) the European Centre for Medium Range Weather Forecasts (ECMWF) Reanalysis version 5 (ERA5)[64], (2) the Japanese 55 year Reanalysis (JRA55)[65], (3) the Modern Era Retrospective Analysis for Research and Applications, version 2 (MERRA2)[66], (4) the NCEP-DOE Reanalysis II (NCEP2)[67], and (5) the National Centers for Environmental Prediction Climate Forecast System Reanalysis (CFSR)[68]. The monthly averaged snowfall and snow cover data used in this study are from the ERA5-Land dataset[69].

Definition of SST index

The IOBM is the leading mode of interannual SST variability over the tropical Indian Ocean on interannual time scales. The IOBM index is defined as the area-weighted mean SST anomaly over 20°S-20°N, 40°E-110°E (Supplementary Fig. 1), with the climatological mean SST during the period of 1979–2020 removed. The Niño 3.4 index is defined as the SST anomaly averaged over 5°N-5°S, 170°W-120°W.

Regression analysis and significance level

In this study, we use a linear regression analysis to examine the linkage between the tropical Indian Ocean variability and North American wintertime climate changes. In particular, a partial regression analysis is applied to remove the ENSO influence in the reanalysis datasets through Gram–Schmidt orthogonalization[70]. We have standardized the IOBM and Niño 3.4 time series before these regressions. The Student's t test is used to assess the statistical significance level. Given the multiple testing problem and spatial autocorrelation, we further conduct field significance test[46] by calculating adjusted p-values according to the control of false discovery rate (FDR) method. We display local significant grid points with black circles that satisfy the FDR criterion in the linear partial regression patterns of Figs. 1 and 4.

Wave activity flux

The wave activity flux proposed by Takaya and Nakamura[71] is utilized to investigate the propagation characteristics of stationary Rossby wave trains. This wave activity flux is typically parallel to the local group velocity of the stationary Rossby wave train. The formula for the horizontal component of the wave activity flux is as follows:

$$\mathbf{W} = \frac{p}{2|\mathbf{U}|}\begin{bmatrix} U\left(\psi_x'^2 - \psi'\psi'_{xx}\right) + V\left(\psi'_x\psi'_y - \psi'\psi'_{xy}\right) \\ U\left(\psi'_x\psi'_y - \psi'\psi'_{xy}\right) + V\left(\psi_y'^2 - \psi'\psi'_{yy}\right) \end{bmatrix}, \quad (1)$$

Here, ψ' represents the perturbed geostrophic streamfunction; $\mathbf{U} = (U, V)$ denotes the climatological mean of horizontal wind velocity during DJF from 1979 to 2020; The pressure, p, is standardized by 1000 hPa.

Sen's slope method and Mann–Kendall test

Sen's slope[72] method is used to calculate the simulated multi-decadal trends of the SAT, the SLP, and the GPH, and the Mann-Kendall test is used to estimate the confidence intervals[72] of trends.

CAM5 model experiment

The National Center for Atmospheric Research (NCAR) atmospheric model, the Community Atmosphere Model version 5 (CAM5)[73], is used to identify the atmospheric responses to the Indian Ocean SST forcing. The CAM5 is the atmospheric component of the Community Earth System Model (CESM), with a horizontal resolution of 2.5° × 1.9° and 26 vertical layers.

The HadISST is used as the lower boundary condition of the atmospheric model. The model experiment is forced by the observed monthly SST over the tropical Indian Ocean (north of 20°S) from 1979 to 2020, with linear buffer zones extending from 20°S to 30°S over the Indian Ocean basin. The sea ice concentration and the SSTs outside the target region are set to the climatological mean state during the period of 1981–2010 with an annual cycle. Other forcings, including the greenhouse gas concentration, aerosols, and solar radiation, are all set to fixed values during the entire integration period. We perform an ensemble experiment with 12 ensemble members driven by the same external forcing, but starting from different initial conditions. The ensemble mean of these simulation results is considered to be the CAM5 response to the observed Indian Ocean SST variability.

GFDL dry-dynamical-core experiment

We use the dry spectral dynamical core of the Geophysical Fluid Dynamics Laboratory (GFDL) atmospheric general circulation model[74] to investigate the evolution of the atmospheric response to Indian Ocean warming. The model is run at triangular 42 horizontal resolution with 19 vertical levels. The model is initialized with the winter climatological background flow of the ERA5 reanalysis in the DJF season and is run with an additional forcing that makes the initial background flow as the balanced state of the model. This additional forcing is obtained by integrating the model with the background flow for a few time steps[56,75]. Once the model is balanced by the background flow, a convective heating is introduced to the thermodynamic energy equation for the first 5 days to mimic the tropical Indian Ocean warming as shown in Fig. 4 of Li, Holland[57]. Temporally, the convective heating is ramped up from day 0 to day 1, maintained for 5 days, and ramped down from day 5 to day 6. Horizontally, the heating follows a cosine function in both latitude and longitude direction, centered at 0°, 67.5°E. The latitude and longitude widths are set to 20° and 45°, respectively, to cover the tropical Indian Ocean[57]. Vertically, the heating is maximized at 500 hPa with a magnitude of 1×10^{-4} K·s^{-1} and extends between 100–1000 hPa following a cosine function. The model is run for 20 days, and the Supplementary Fig. 9 shows the dynamical response to an initial perturbation mimicking the tropical Indian Ocean warming at day 13.

Data availability

All observational and reanalysis data used in this study are obtained from publicly available sources. The HadISST data is available at https://www.metoffice.gov.uk/hadobs/hadisst/data/download.html. The outgoing longwave radiation data is available at https://iridl.ldeo.columbia.edu/SOURCES/.NOAA/.NCEP/.CPC/.GLOBAL/.monthly/.olr/index.html. The ERA5 reanalysis data is available at https://www.ecmwf.int/en/forecasts/datasets/. The JRA55 reanalysis data is available at https://rda.ucar.edu/datasets/ds628.1/dataaccess/. The MERRA2 reanalysis data is available at https://disc.gsfc.nasa.gov/datasets/. The NCEP2 reanalysis data is available at https://psl.noaa.gov/data/gridded/data.ncep.reanalysis2.html. The data generated in the analyses is provided in the Source Data file. The model output data

in this study is available from the corresponding author upon request. Source data are provided with this paper.

Code availability

The data in this study are analyzed with MATLAB, available at https://in.mathworks.com/products/matlab.html. The code of the CESM1 model used is available at http://www.cesm.ucar.edu/models/cesm1.2. The code of the GFDL model is available at https://www.gfdl.noaa.gov/atmospheric-model/. Other codes used in the analyses are available from the corresponding author upon request.

References

1. Doss-Gollin, J., Farnham, D. J., Lall, U. & Modi, V. How unprecedented was the February 2021 Texas cold snap? *Environ. Res. Lett.* **16**, 064056 (2021).
2. Matthias, V. & Kretschmer, M. The influence of stratospheric wave reflection on North American cold spells. *Mon. Weather Rev.* **148**, 1675–1690 (2020).
3. Palmer, T. Record-breaking winters and global climate change. *Science* **344**, 803–804 (2014).
4. Déry S. J., Brown R. D. Recent Northern Hemisphere snow cover extent trends and implications for the snow-albedo feedback. *Geophys. Res. Lett.* **34**, L22504 (2007).
5. Diro, G. & Sushama, L. Contribution of snow cover decline to projected warming over North America. *Geophys. Res. Lett.* **47**, e2019GL084414 (2020).
6. Sedlar, J. et al. A transitioning Arctic surface energy budget: the impacts of solar zenith angle, surface albedo and cloud radiative forcing. *Clim. Dyn.* **37**, 1643–1660 (2011).
7. Hou, Y. et al. Cold Springs Over Mid-Latitude North America Induced by Tropical Atlantic Warming. *Geophys. Res. Lett.* **50**, e2023GL104180 (2023).
8. Yu, B., Li, G., Chen, S. & Lin, H. The role of internal variability in climate change projections of North American surface air temperature and temperature extremes in CanESM2 large ensemble simulations. *Clim. Dyn.* **55**, 869–885 (2020).
9. Kamae, Y. et al. Forced response and internal variability of summer climate over western North America. *Clim. Dyn.* **49**, 403–417 (2017).
10. Hoerling, M., Eischeid, J. & Perlwitz, J. Regional precipitation trends: Distinguishing natural variability from anthropogenic forcing. *J. Clim.* **23**, 2131–2145 (2010).
11. Jones, G. S., Stott, P. A. & Christidis, N. Attribution of observed historical near–surface temperature variations to anthropogenic and natural causes using CMIP5 simulations. *J. Geophys. Res. Atmos.* **118**, 4001–4024 (2013).
12. Simmons, A., Wallace, J. & Branstator, G. Barotropic wave propagation and instability, and atmospheric teleconnection patterns. *J. Atmos. Sci.* **40**, 1363–1392 (1983).
13. Held, I. M., Lyons, S. W. & Nigam, S. Transients and the extratropical response to El Niño. *J. Atmos. Sci.* **46**, 163–174 (1989).
14. Sigmond, M. & Fyfe, J. C. Tropical Pacific impacts on cooling North American winters. *Nat. Clim. Change* **6**, 970–974 (2016).
15. Wallace, J. M. & Gutzler, D. S. Teleconnections in the geopotential height field during the Northern Hemisphere winter. *Mon. Weather Rev.* **109**, 784–812 (1981).
16. Klein, S. A., Soden, B. J. & Lau, N.-C. Remote sea surface temperature variations during ENSO: Evidence for a tropical atmospheric bridge. *J. Clim.* **12**, 917–932 (1999).
17. Alexander, M. A. et al. The atmospheric bridge: The influence of ENSO teleconnections on air–sea interaction over the global oceans. *J. Clim.* **15**, 2205–2231 (2002).
18. Liu, Z. et al. Recent contrasting winter temperature changes over North America linked to enhanced positive Pacific-North American pattern. *Geophys. Res. Lett.* **42**, 7750–7757 (2015).
19. Kushnir, Y., Seager, R., Ting, M., Naik, N. & Nakamura, J. Mechanisms of tropical Atlantic SST influence on North American precipitation variability. *J. Clim.* **23**, 5610–5628 (2010).
20. Peng S., Robinson W. A., Li S. North Atlantic SST forcing of the NAO and relationships with intrinsic hemispheric variability. *Geophys. Res. Lett.* **29**, 117-111-117-114 (2002).
21. Ning, L. & Bradley, R. S. Winter climate extremes over the northeastern United States and southeastern Canada and teleconnections with large-scale modes of climate variability. *J. Clim.* **28**, 2475–2493 (2015).
22. Hou, Y. et al. A surface temperature dipole pattern between Eurasia and North America triggered by the Barents–Kara sea-ice retreat in boreal winter. *Environ. Res. Lett.* **17**, 114047 (2022).
23. Ting, M. & Sardeshmukh, P. D. Factors determining the extratropical response to equatorial diabatic heating anomalies. *J. Atmos. Sci.* **50**, 907–918 (1993).
24. Molteni, F., Stockdale, T. N. & Vitart, F. Understanding and modelling extra-tropical teleconnections with the Indo-Pacific region during the northern winter. *Clim. Dyn.* **45**, 3119–3140 (2015).
25. Molteni, F. et al. Boreal-winter teleconnections with tropical Indo-Pacific rainfall in HighResMIP historical simulations from the PRIMAVERA project. *Clim. Dyn.* **55**, 1843–1873 (2020).
26. Hu, Z.-Z., Kumar, A., Jha, B., Chen, M., Wang, W. The tropical Indian Ocean matters for US winter precipitation variability and predictability. *Environ. Res. Lett.* **18**, 074033 (2023).
27. Abid, M. A., Kucharski, F., Molteni, F. & Almazroui, M. Predictability of Indian Ocean precipitation and its North Atlantic teleconnections during early winter. *npj Clim. Atmos. Sci.* **6**, 17 (2023).
28. Stan, C. et al. Review of tropical-extratropical teleconnections on intraseasonal time scales. *Rev. Geophys.* **55**, 902–937 (2017).
29. Lin, H. & Brunet, G. The influence of the Madden–Julian oscillation on Canadian wintertime surface air temperature. *Mon. Weather Rev.* **137**, 2250–2262 (2009).
30. Lin, H., Brunet, G. & Mo, R. Impact of the Madden–Julian oscillation on wintertime precipitation in Canada. *Mon. Weather Rev.* **138**, 3822–3839 (2010).
31. Zhou, S., L'Heureux, M., Weaver, S. & Kumar, A. A composite study of the MJO influence on the surface air temperature and precipitation over the continental United States. *Clim. Dyn.* **38**, 1459–1471 (2012).
32. Hoskins, B. J. & Karoly, D. J. The steady linear response of a spherical atmosphere to thermal and orographic forcing. *J. Atmos. Sci.* **38**, 1179–1196 (1981).
33. Hoskins, B. J., James, I. N. & White, G. H. The shape, propagation and mean-flow interaction of large-scale weather systems. *J. Atmos. Sci.* **40**, 1595–1612 (1983).
34. Jin, F. & Hoskins, B. J. The direct response to tropical heating in a baroclinic atmosphere. *J. Atmos. Sci.* **52**, 307–319 (1995).
35. Trenberth, K. E. et al. Progress during TOGA in understanding and modeling global teleconnections associated with tropical sea surface temperatures. *J. Geophys. Res. Oceans* **103**, 14291–14324 (1998).
36. Saji, N., Xie, S. & Yamagata, T. Tropical Indian Ocean variability in the IPCC twentieth-century climate simulations. *J. Clim.* **19**, 4397–4417 (2006).
37. Yang, J., Liu, Q., Xie, S. P., Liu, Z. & Wu, L. Impact of the Indian Ocean SST basin mode on the Asian summer monsoon. *Geophys. Res. Lett.* **34**, L02708 (2007).
38. Xie, S.-P. et al. Indian Ocean capacitor effect on Indo–western Pacific climate during the summer following El Niño. *J. Clim.* **22**, 730–747 (2009).
39. Lau, N.-C. & Nath, M. J. Atmosphere–ocean variations in the Indo-Pacific sector during ENSO episodes. *J. Clim.* **16**, 3–20 (2003).

40. Kug, J.-S. & Kang, I.-S. Interactive feedback between ENSO and the Indian Ocean. *J. Clim.* **19**, 1784–1801 (2006).
41. Du, Y., Xie, S.-P., Huang, G. & Hu, K. Role of air–sea interaction in the long persistence of El Niño–induced north Indian Ocean warming. *J. Clim.* **22**, 2023–2038 (2009).
42. Kumar, A. & Hoerling, M. P. Specification of regional sea surface temperatures in atmospheric general circulation model simulations. *J. Geophys. Res.: Atmos.* **103**, 8901–8907 (1998).
43. Annamalai, H., Okajima, H. & Watanabe, M. Possible impact of the Indian Ocean SST on the Northern Hemisphere circulation during El Niño. *J. Clim.* **20**, 3164–3189 (2007).
44. Rao, J. & Ren, R. A decomposition of ENSO's impacts on the northern winter stratosphere: Competing effect of SST forcing in the tropical Indian Ocean. *Clim. Dyn.* **46**, 3689–3707 (2016).
45. Cai, W. et al. Pantropical climate interactions. *Science* **363**, eaav4236 (2019).
46. Wilks, D. The stippling shows statistically significant grid points": How research results are routinely overstated and overinterpreted, and what to do about it. *Bull. Am. Meteorol. Soc.* **97**, 2263–2273 (2016).
47. Deser, C., Simpson, I. R., Phillips, A. S. & McKinnon, K. A. How well do we know ENSO's climate impacts over North America, and how do we evaluate models accordingly? *J. Clim.* **31**, 4991–5014 (2018).
48. Park, C. H. et al. Sub-Seasonal Variability of ENSO Teleconnections in Western North America and Its Prediction Skill. *J. Geophys. Res.: Atmos.* **128**, e2022JD037985 (2023).
49. Hoskins, B. J. & Ambrizzi, T. Rossby wave propagation on a realistic longitudinally varying flow. *J. Atmos. Sci.* **50**, 1661–1671 (1993).
50. Hansen, J., Ruedy, R., Sato, M. & Lo, K. Global surface temperature change. *Rev. Geophys.* **48**, RG4004 (2010).
51. Kosaka, Y. & Xie, S.-P. Recent global-warming hiatus tied to equatorial Pacific surface cooling. *nature* **501**, 403–407 (2013).
52. Dong, B. & Dai, A. The influence of the interdecadal Pacific oscillation on temperature and precipitation over the globe. *Clim. Dyn.* **45**, 2667–2681 (2015).
53. Meehl, G. A., Hu, A., Santer, B. D. & Xie, S.-P. Contribution of the Interdecadal Pacific Oscillation to twentieth-century global surface temperature trends. *Nat. Clim. Change* **6**, 1005–1008 (2016).
54. Li, X., Holland, D. M., Gerber, E. P. & Yoo, C. Impacts of the north and tropical Atlantic Ocean on the Antarctic Peninsula and sea ice. *Nature* **505**, 538–542 (2014).
55. Li, X., Xie, S.-P., Gille, S. T. & Yoo, C. Atlantic-induced pan-tropical climate change over the past three decades. *Nat. Clim. Change* **6**, 275–279 (2016).
56. Yoo, C., Lee, S. & Feldstein, S. B. Arctic response to an MJO-like tropical heating in an idealized GCM. *J. Atmos. Sci.* **69**, 2379–2393 (2012).
57. Li, X., Holland, D. M., Gerber, E. P. & Yoo, C. Rossby waves mediate impacts of tropical oceans on West Antarctic atmospheric circulation in austral winter. *J. Clim.* **28**, 8151–8164 (2015).
58. Park, M. & Lee, S. Relationship between tropical and extratropical diabatic heating and their impact on stationary–transient wave interference. *J. Atmos. Sci.* **76**, 2617–2633 (2019).
59. Nitta, T. Convective activities in the tropical western Pacific and their impact on the Northern Hemisphere summer circulation. *J. Meteorological Soc. Jpn. Ser. II* **65**, 373–390 (1987).
60. Karoly, D. J. Southern hemisphere circulation features associated with El Niño-Southern Oscillation events. *J. Clim.* **2**, 1239–1252 (1989).
61. Cohen, J. L., Furtado, J. C., Barlow, M. A., Alexeev, V. A. & Cherry, J. E. Arctic warming, increasing snow cover and widespread boreal winter cooling. *Environ. Res. Lett.* **7**, 014007 (2012).
62. Rayner, N., et al. Global analyses of sea surface temperature, sea ice, and night marine air temperature since the late nineteenth century. *J. Geophys. Res. Atmos.* **108**, 4407 (2003).
63. Liebmann, B. & Smith, C. A. Description of a complete (interpolated) outgoing longwave radiation dataset. *Bull. Am. Meteorol. Soc.* **77**, 1275–1277 (1996).
64. Hersbach, H. et al. The ERA5 global reanalysis. *Q. J. R. Meteorol. Soc.* **146**, 1999–2049 (2020).
65. Kobayashi, S. et al. The JRA-55 reanalysis: general specifications and basic characteristics. *J. Meteorological Soc. Jpn. Ser. II* **93**, 5–48 (2015).
66. Gelaro, R. et al. The modern-era retrospective analysis for research and applications, version 2 (MERRA-2). *J. Clim.* **30**, 5419–5454 (2017).
67. Kanamitsu, M. et al. Ncep–doe amip-ii reanalysis (r-2). *Bull. Am. Meteorol. Soc.* **83**, 1631–1644 (2002).
68. Saha, S. et al. The NCEP climate forecast system reanalysis. *Bull. Am. Meteorol. Soc.* **91**, 1015–1058 (2010).
69. Muñoz-Sabater, J. et al. ERA5-Land: A state-of-the-art global reanalysis dataset for land applications. *Earth Syst. Sci. Data* **13**, 4349–4383 (2021).
70. Björck, Å. Numerics of gram-schmidt orthogonalization. *Linear Algebra Appl.* **197**, 297–316 (1994).
71. Takaya, K. & Nakamura, H. A formulation of a phase-independent wave-activity flux for stationary and migratory quasigeostrophic eddies on a zonally varying basic flow. *J. Atmos. Sci.* **58**, 608–627 (2001).
72. Gocic, M. & Trajkovic, S. Analysis of changes in meteorological variables using Mann-Kendall and Sen's slope estimator statistical tests in Serbia. *Glob. Planet. Change* **100**, 172–182 (2013).
73. Neale, R. B. et al. Description of the NCAR community atmosphere model (CAM 5.0). *NCAR Tech. Note NCAR/TN-486+ STR* **1**, 1–12 (2010).
74. Held, I. M. & Suarez, M. J. A proposal for the intercomparison of the dynamical cores of atmospheric general circulation models. *Bull. Am. Meteorol. Soc.* **75**, 1825–1830 (1994).
75. Franzke, C., Lee, S. & Feldstein, S. B. Is the North Atlantic Oscillation a breaking wave? *J. Atmos. Sci.* **61**, 145–160 (2004).

Acknowledgements

Y.H. and X.L. were supported by the National Science Fund for Distinguished Young Scholars (42325605) and the National Natural Science Foundation of China (42176243). N.C.J. was supported by the National Oceanic and Atmospheric Administration to the Geophysical Fluid Dynamics Laboratory. C.W. was supported by the National Natural Science Foundation of China (42192564 and W2441014). W.S. was supported by Taishan Scholars Program of Shandong Province (tsqn202312158). We thank Dr. Liwei Jia for constructive comments on an earlier version of the manuscript. We acknowledge the High Performance Computer resources/Earth System Model Software/2024-EL-ZD-000191 from the National Key Scientific and Technological Infrastructure project "Earth System Numerical Simulation Facility" (EarthLab).

Author contributions

Y.H., X.L., S.-P.X., and N.C.J. designed the research. Y.H. performed the data analysis, ran the CAM5 simulations, and prepared figures. C.Y. ran the GFDL model experiments. Y.H., X.L., S.-P.X., N.C.J., C.W., C.Y., K.D., and W.S. contributed to the writing and reviewing of the paper.

Competing interests

The authors declare no competing interests.

Additional information

Supplementary information The online version contains supplementary material available at https://doi.org/10.1038/s41467-024-53921-y.

Correspondence and requests for materials should be addressed to Xichen Li.

Peer review information *Nature Communications* thanks the anonymous reviewers for their contribution to the peer review of this work. A peer review file is available.